Desalination and Water Treatment
www.deswater.com

doi: 10.5004/dwt.2017.21829

100 (2017) 55–66
December

Removal of lead ions from wastewater using multi walled carbon nanotubes modified with sodium lauryl sulfate

Malaz M. Suliman[a], Taleb H. Ibrahim[a,*], Fawwaz Jumean[b], Mustafa I. Khamis[b], Muhammad A. Sabri[a]

[a]*Department of Chemical Engineering, American University of Sharjah, Tel. +971 6 5152460, Fax +971 6 5152979, email: italeb@aus.edu*
[b]*Department of Chemistry, Biology and Environmental Sciences, American University of Sharjah, P.O. Box 26666 Sharjah, UAE*

Received 7 September 2017; Accepted 19 December 2017

ABSTRACT

Multi walled carbon nanotubes (MWCNTs) modified with sodium lauryl sulfate (SLS) were synthesized, characterized and successfully used for the removal of Pb^{2+} from aqueous solutions. Adsorption results revealed that this surface modification increased adsorption capacity from 3.84 to 141 mg/g. Adsorption on raw-MWCNTs followed the Langmuir isotherm with q_m = 3.84 mg/g and K_L = 0.29 L/mg, whereas adsorption on SLS-MWCNTs followed the Freundlich isotherm with n = 2.50 and K_F = 15.40 $mg^{0.6}{\cdot}L^{0.4}$/g. Adsorption kinetics on raw and modified MWCNTs followed a pseudo second order law with rate constants 0.11 and 0.06 g/mg·min, respectively. Thermodynamic studies showed that Pb^{2+} was physisorbed on both adsorbents, with apparent Gibbs free energy, ΔG°, values of –0.45 and –9.21 kJ/mol at 25°C, respectively. Magnetite derivatives of SLS-MWCNTs were synthesized and used for Pb^{2+} removal. Batch adsorption studies on the magnetite and non-magnetite SLS-MWCNTs gave similar results. The enhanced density of the magnetite pellets of SLS-MWCNTs allowed for their use in a packed bed column. Column operation modeling results showed that the modified dose response model most adequately describes the column data with parameter values q_{mdr} = 28.4 mg/g and a' = 3.47 mg^{-1}.

Keywords: Multi walled carbon nanotubes; Sodium lauryl sulfate; Lead; Adsorption

1. Introduction

Recently, carbon nanotubes (CNTs) have been employed extensively as new adsorbents for the removal of a number of pollutants. CNTs have large surface areas with hollow, porous and layered structures that make them potentially effective adsorbents [1]. However, a major problem of carbon nanotubes is their tendency, driven by van der Waals forces, to agglomerate and form bundles in aqueous solutions [1,2]. This behavior can cause difficulties in CNTs dispersion. However, the problem can be resolved by surface modifications that reduce accumulation of CNTs and consequently enhance their dispersion in different media. Moreover, such modifications can increase adsorption capacity for pollutants [1,2].

Surface modification can be done using either of two main methods. The covalent method can be used to attach the desired functional group permanently to the surface of nanotubes. In this method, groups are chemically bound to the surface, with the possibility of causing defects in the structure of the CNTs, thereby affecting their original properties [3,4]. Moreover, large amounts of chemicals are used in this method, thus possibly harming the environment [2]. In the non-covalent method, functional groups are only physically, or weakly, bound to the surface [4]. This method is important and very common because it does not damage the structure or substantially affect CNTs properties [3]. Examples of non-covalent functionalization include wrapping of polymer chains around the nanotubes

*Corresponding author.

and adsorption of surfactants on the surface [4]. Surfactants are adsorbed on the surface of raw carbon nanotubes through their hydrophobic chains, thereby making nanotubes hydrophilic and dispersible in aqueous solutions [2]. Carbon nanotubes functionalization was considered by many researchers. Examples of reported functional groups include magnetic hydroxypropyl chitosan [5], 2-vinylpyridine (VP) [6], titanium dioxide [7], tris (2-aminoethyl) amine [8], 1-isatin-3-thiosemicarbazone [9], thiol [10], manganese oxide [11] and concentrated nitric acid [12].

One limitation of the application of CNTs and their organic surface modification arises from their very light weight, which limits their application in fixed bed columns under normal conditions. It is thus important to devise a process for making them denser and consequently stable when packed in a column. Magnetation is an efficient way to make carbon nanotubes heavier and granular. In previous studies, thiol-groups grafted on the surface of CNTs/Fe_3O_4 nanocomposites [10] and magnetic hydroxypropyl chitosan/oxidized multi walled carbon nanotubes composites were used for Pb^{2+} removal [13].

In this work, the efficiency of using sodium lauryl sulfate modified multi walled carbon nanotubes (SLS-MWCNTs) as adsorbents in the removal of Pb^{2+} from aqueous solutions was studied and compared to that obtained with raw-MWCNTs. Moreover, equilibrium, kinetics, mechanistic and thermodynamics studies were carried out for both adsorbents. Furthermore, both magnetization and surface modification were applied to raw MWCNTs. Magnetite pellets of MWCNTs modified with sodium lauryl sulfate (SLS-MWCNTs-magnetite) were synthesized, characterized and used for Pb^{2+} removal in batch mode experiments. The results were compared to those without magnetite. Moreover, SLS-MWCNTs-magnetite were used in packed bed column.

2. Experimental

2.1. Materials

Multi walled carbon nanotubes (>95% purity) with less than 8 nm diameter and 10–30 μm length were obtained from Grafen Chemical Industries (KNT-M31, Turkey). All chemicals were of analytical grade. Sodium lauryl sulfate (SLS) was from Daejung Chemicals & Metals (South Korea) and lead nitrate from Pharmacos (England). Ferrous sulfate heptahydrate, from Fluka (Germany) and ferric chloride hexahydrate, from Panreac (Spain) were used without further purification to prepare magnetite nanotubes. Doubly distilled water (DDW) was used throughout. 1.0 M HNO_3 and 1.0 M NaOH were used for pH adjustment.

2.2. Instrumentation

DDW was generated using an Aquatron A4000D (UK) water still. Samples were shaken in a temperature controlled flask shaker (Edmund Buhler, Germany). 0.45 μm syringe filters were used (MCE Membrane, Membrane Solutions, USA). pH measurements were conducted on an Orion 210A$^+$ pH meter (ThermoElectron, USA). [Pb^{2+}] was measured using either an inductively *coupled plasma* optical emission spectrometer (Varian sequential *ICP*-OES, USA) or an atomic absorption spectrometer (SpectraAA 220FS Varian, USA). An ultrasonication bath (Elma, Germany) was used to obtain surfactant-coated MWCNTs. The modified adsorbent was centrifuged (HERMLE Labortechnik, Germany). A hot box oven with fan (Gallenkamp, UK) and a vacuum oven (Wisd Laboratory Instruments, Ireland) were used for drying. MWCNTs were characterized using an energy dispersive X-ray spectroscopy EDS detector (Oxford instruments, UK), a thermogravimetric analyzer TGA (PerkinElmer, USA) and a Fourier transform infrared spectrometer (PerkinElmer, USA). Surface area and pore size characterization were done on Quantachrome gas sorption analyzer (Autosorb iQ, USA), using nitrogen adsorption and desorption isotherms at 77 K. Zeta potential measurements were conducted on Anton Paar Litesizer 500 (Australia).

2.3. Synthesis of SLS-MWCNTs

In order to modify the MWCNTs surface with SLS, 0.5 g of raw MWCNTs was added to 500 ml of 8 mM SLS aqueous solution. A well-dispersed SLS-MWCNTs suspension was obtained after ultrasonication at 144 W for 2 h. The dispersion was then centrifuged at 4000 rpm for 15 min and pellets were obtained. Finally, SLS-modified MWCNTs were obtained after drying the pellets for 2 h at 110°C in the hot box oven followed by vacuum drying for 48 h at 60°C.

2.4. Synthesis of magnetite SLS-MWCNTs

Magnetite pellets of raw MWCNTs were prepared following the procedure developed by Kerkez et al. [14]. SLS modification was then carried out following the procedure described in Section 2.3.

2.5. Batch experiments

The effect of adsorbent dosage, contact time and solution pH on removal efficiency was studied using batch mode adsorption experiments. The effect of each parameter was followed by varying it while keeping all other parameters fixed and observing the change in removal percentage, as calculated from Eq. (1). The optimum value of a parameter was then used in further experiments.

$$Removal\ \% = \frac{C_o - C_e}{C_o} \times 100 \quad (1)$$

where C_o and C_e are the initial and equilibrium concentrations, respectively (ppm). For adsorption experiments, 1000 ppm stock Pb^{2+} solution was prepared and the required dilutions were made. pH was adjusted using 1.0 M HNO_3 and 1.0 M NaOH. Known masses of MWCNTs were separately added to 10 ml aliquots then placed in the thermostated shaker at 150 rpm. After shaking for a predetermined time interval, samples were filtered using 0.45 μm syringe filters. Final [Pb^{2+}] was measured using either ICP or AA. Glassware were repeatedly cleaned using 15% nitric acid then washed thoroughly with DDW before drying.

2.6. Fixed bed column operation

For column operation, magnetite SLS-MWCNTs were packed in a glass column of 50 cm length and 1.0 cm internal diameter. The height of the bed, supported by glass wool, was kept at 2.0 cm. The column was loaded with 100 ppm Pb^{2+} solution, percolated under gravity at a flow rate of 1.0 ml/min. Samples were collected for analysis at different intervals.

2.7. Modeling for fixed bed column operation

It is essential to predict the performance of fixed bed column under different conditions. Since experimental determinations are expensive and time-consuming, it is convenient to use mathematical models to determine the best operating conditions and to optimize the design of packed bed columns [15]. Data collected from the operation of the fixed bed column were fitted to the following models:

2.7.1. Thomas model

This is a frequently used model to predict the adsorption capacity of adsorbents in columns. It is based on the Langmuir isotherm, assumes second order kinetics and negligible internal and external diffusion resistances [15]. The model is expressed by Eq. (2) [7]:

$$ln\left[\frac{C_o}{C_t}-1\right]=\frac{kTh*q*m}{Q}-k_{th}C_o t \quad (2)$$

where C_t is the concentration at time t (mg/L), k_{Th} is the Thomas kinetic coefficient (ml/min·mg), q is the adsorption capacity (mg/g), m is the mass of adsorbent in the column and Q is the fluid volumetric flow rate (ml/min). k_{Th} and q_o can be calculated from the slope and intercept of ln [(C_o/C_t) – 1] *vs* t [16].

2.7.2. Yoon–Nelson model

This is a simple model that is applicable to one component systems. It requires fewer column data than other models and can predict the time required for 50% column breakthrough without the need to run prolonged column experiments. However, it is not suitable for predicting process variables [15,16]. This model follows Eq. (3) [16]:

$$ln\left[\frac{C_t}{C_o-C_t}\right]=k_{YN}t-\tau k_{YN} \quad (3)$$

where k_{YN} is the Yoon-Nelson rate constant (min^{-1}) and t is the time required for 50% column breakthrough (min). k_{Th} and t can be found from a plot of ln [C_t/ C_o – C_t] vs t [16].

2.7.3. Adam–Bohart model

This model is based on surface reaction theory and assumes that the reaction is not immediate. It is convenient in describing the initial part of column operation and is expressed by Eq. (4) [16]:

$$\ln\frac{C_t}{C_o}=k_{AB}C_o t-\frac{k_{AB}N_o z}{U_o} \quad (4)$$

where k_{AB} is the Adam-Bohart kinetic constant (L/mg·min), N_o is the saturation concentration (mg/L), z is the bed height (cm) and U_o is the velocity calculated from the volumetric flow rate over the column cross section area (cm/min). k_{AB} and N_o can be found by plotting ln [C_t/C_o] vs. t [16].

2.7.4. Modified dose response model (MDR)

This model was developed originally for pharmacology studies and has recently been used to describe adsorption of metals [15]. Compared to the Thomas model, MDR is more accurate in predictions of the breakthrough curve at low and high time intervals curve [17]. MDR is expressed by Eq. (5) [15]:

$$\ln\frac{C_t}{C_o-C_t}=a'ln\left(C_o*Q*\ t\right)-a'ln\left(q*m\right) \quad (5)$$

where a' is the MDR constant, obtained by plotting ln [(C_t/C_o) – C_t] vs ln (C_o*Q*t).

3. Results and discussion

3.1. Surface characterization

Surface characterization of raw and SLS modified MWCNTs was conducted using scanning electron microscopy (SEM), energy dispersive spectrometry (EDS), thermogravimetric analysis (TGA), zeta potential, surface area and Fourier transform infrared spectroscopy (FTIR). EDS, TGA and FTIR results are shown in Figs. 1–6.

Fig. 1 displays the SEM image of MWCNT (1a) and SLS-MWCNT (1b) and reveals the morphology changes in the adsorbent's surface changes upon modification with SLS. This observation shows that binding of SLS to the surface of MWCNT lead to this modification.

EDS of raw nanotubes (Fig. 2) shows that carbon, aluminum and iron are present on the surface of the MWCNTs in 96.5, 3.2 and 0.4 wt %, respectively. The presence of small amounts of aluminum and iron is due to metal catalysts used in the synthesis of the MWCNTs. After modification (Fig. 3), the carbon weight percentage on the surface dropped to 80.4%, with sodium and sulfur also present. This confirms that modification was successfully achieved.

TGA results (Fig. 4) also confirmed that the raw MWCNTs have been modified. The behavior of raw and modified nanotubes with increasing temperatures markedly differ. Fig. 4 also shows that the modified nanotubes are stable with no loss in weight, up to 200°C. FTIR results for both raw and SLS-MWCNTs are shown in Fig. 5. Attaching the SLS surfactant to the raw carbon nanotubes resulted in the appearance of new peaks. Those at 1059.02, 1209.91 and 1374.51 cm^{-1} belong to the S=O functional group of sulfur in [$CH_3(CH_2)_{11}SO_4Na$] and those at 2851.64 and 2917.58 cm^{-1} can be attributed to the C-H group in CH_3 and CH_2. The peak at 3406.59 cm^{-1} belongs to the O–H group [18]. In

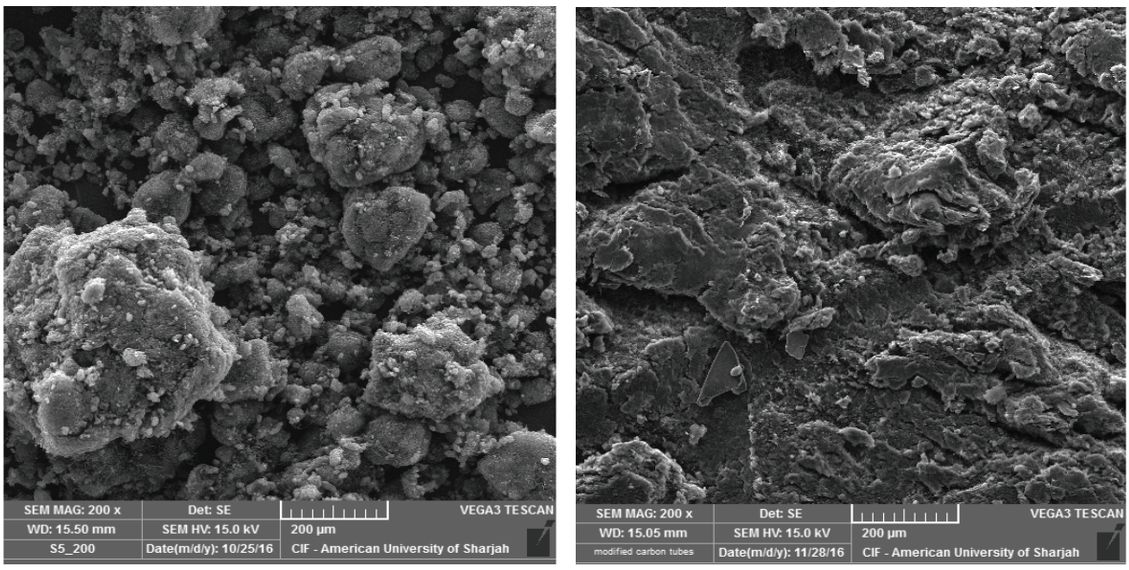

A B

Fig. 1. SEM image of raw-MWCNTs (a) and SLS-MWCNTs (b).

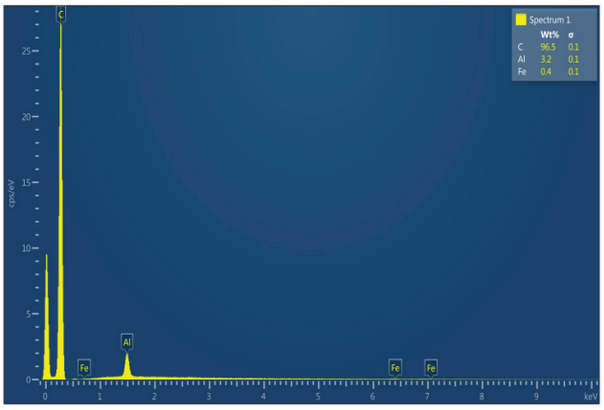

Fig. 2. Energy dispersive spectrometry (EDS) analysis of raw-MWCNTs.

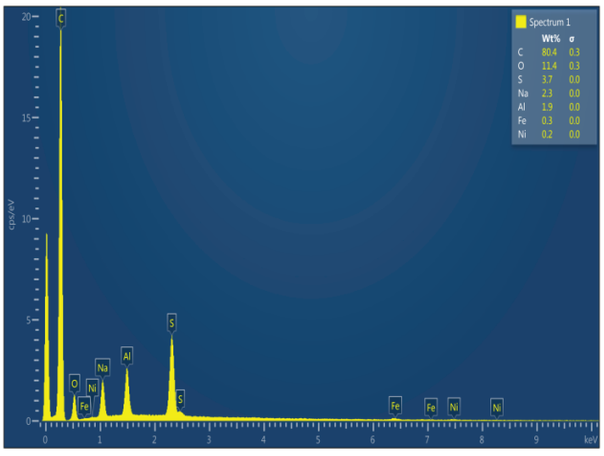

Fig. 3. Energy dispersive spectrometry (EDS) analysis of SLS-MWCNTs.

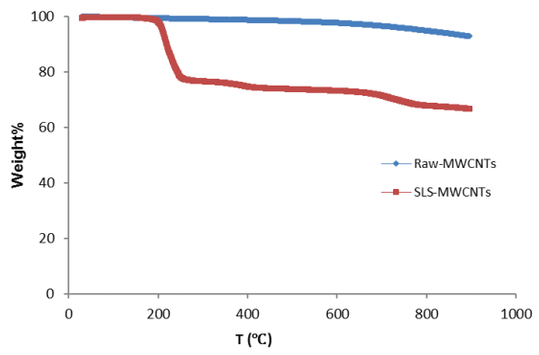

Fig. 4. TGA results of raw and SLS-MWCNTs.

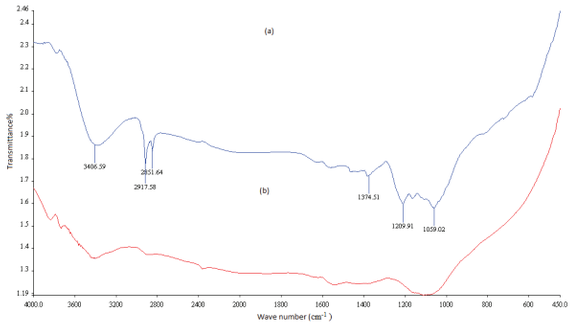

Fig. 5. FTIR results for (a) SLS-MWCNTs and (b) Raw-MWCNTs.

sum, the four characterization techniques employed clearly highlight the difference between the surfaces of raw and SLS-MWCNTs and confirm that surface modification has been successfully achieved.

The magnetite pellets of MWCNTs before and after modification with SLS were characterized using FTIR (Fig. 6).

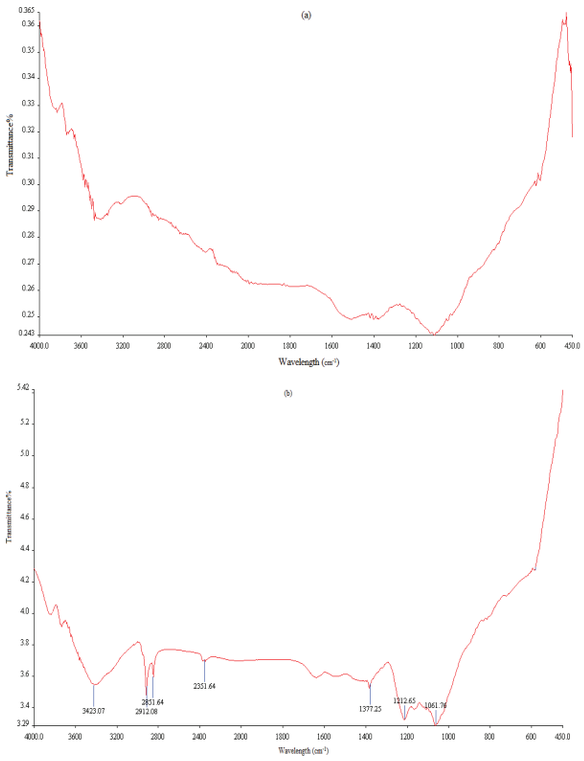

Fig. 6. FTIR results of (a) magnetite raw-MWCNTs and (b) magnetite SLS-MWCNTs.

The peak at 493.89 cm^{-1} in the magnetite raw-MWCNTs spectra belongs to the iron oxide used in magnetization [19]. Attaching the SLS surfactant to the raw magnetite carbon nanotubes resulted in the appearance of the same peaks of the non-magnetite SLS-MWCNTs. The interaction of SLS with MWCN adsorbents probably follows the scheme proposed in Fig. 7. The interaction is based on physical sorption of SLS by the carbon backbone, whereas Pb^{2+} adsorption occurs mainly by an ion exchange mechanism.

Nitrogen adsorption-desorption was carried out in order to determine the pore characteristics of MWCNTs and their derivatives. The isotherms shown in Fig. 8 are type III (multilayer) and indicate that all the samples have macroporous surfaces. The nitrogen uptake was low at low pressure indicating low nitrogen-solid affinity. The results suggest multilayer, rather than monolayer, formation. Fig. 9 shows the pore size distribution (PSD) of MWCNT and its derivatives. The PSD results are consistent with type III isotherm and indicate that the majority of the pores are macroporous, with only a few being mesoporous. Fig. 9 also shows the consistency of the pore structure of samples, before and after being modified with magnetite and SLS.

Table 1 presents the BET surface area and pore volumes of the samples. The BET surface area of MWCNT and magnetite MWCNT are almost identical. Similarly, the BET surface area of SLS-MWCNT and magnetite SLS-MWCNT are identical. The BET surface area, total pore volume and micropore volume decrease when the MWCNT and magnetite MWCNT samples are modified by SLS. This can be due

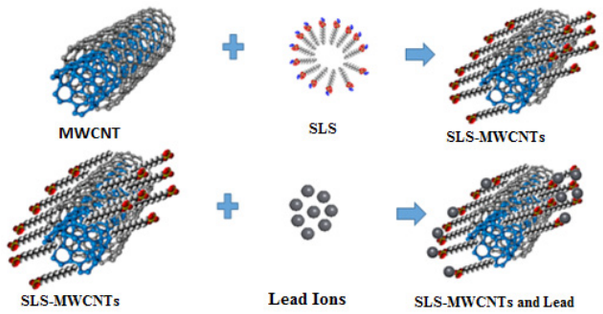

Fig. 7. Schematic representation of the modification of MWCNTs by SLS and the subsequent adsorption of Pb^{2+} by the SLS-MWCNTs complex.

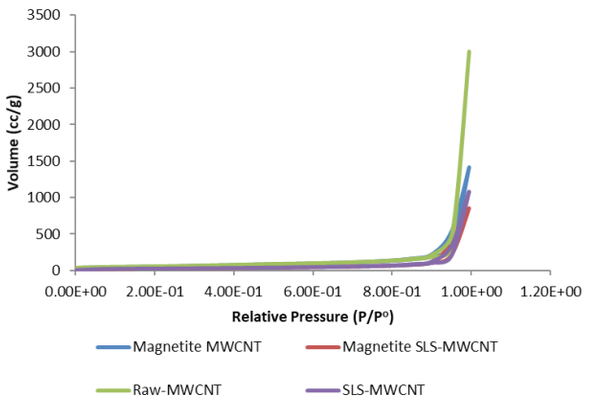

Fig. 8. Nitrogen isotherms at –196°C for raw-MWCNT and its derivatives.

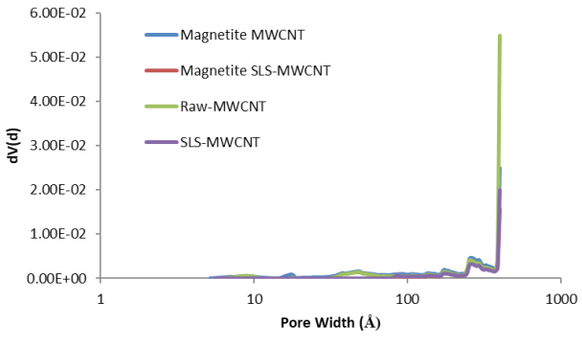

Fig. 9. Pore size characteristics of raw-MWCNT and its derivatives.

to the coating of these samples by SLS, thereby reducing the surface area and the pore volumes.

The zeta potentials of MWCNT and its derivatives are presented in Fig. 10. Inspection of the results reveals that its value for MWCNT is positive at pH 6.5 with isoelectronic point at pH 3.2. All other samples show negative zeta potentials, with that for SLS-MWCNT being the highest at pH 6.5. These results contribute to explaining why the affinity of these adsorbents towards Pb^{2+} removal from industrial wastewater is pH dependent.

Table 1
BET surface area and pore characteristics of MWCNT and its derivatives

Samples	Surface area (m^2/g)	DFT V<20	DFT Vtotal
CNTMW	191.022	1.74E-03	1.34E+00
Magnetite-MWCNT	184.794	3.81E-03	1.04E+00
SLS-MWCNT	91.717	0.00E+00	7.02E-01
Magnetite SLS-MWCNT	88.702	0.00E+00	6.80E-01

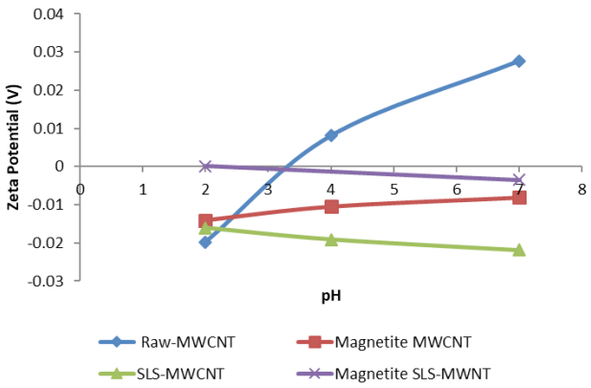

Fig. 10. Zeta potential of raw-MWCNT and its derivatives at different pH. The results are average of 1000 runs with maximum standard deviation of ± 0.0005 V. The adjusted voltage is 200 V at 25.0°C.

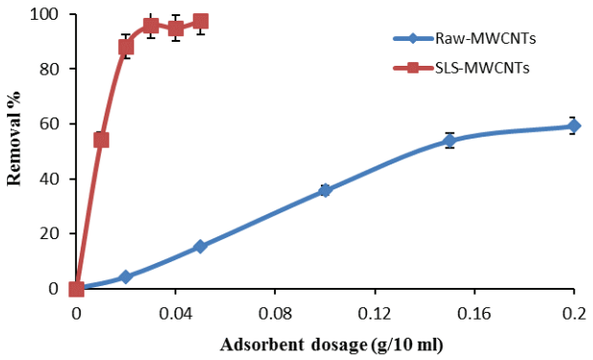

Fig. 11. Effect of adsorbent dosage on the removal of Pb^{2+} from aqueous solutions for raw and SLS-MWCNTs at initial concentration = 100 ppm, pH = 5.30 ± 0.05, T = 25.0 ± 0.2°C, contact time = 120 min and shaking rate = 150 rpm.

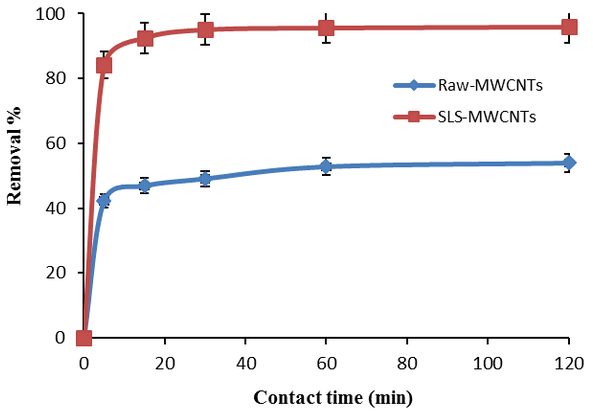

Fig. 12. Effect of contact time on the removal of Pb^{2+} from aqueous solutions for raw and SLS-MWCNTs. Initial adsorbent concentration = 100 ppm, pH = 5.30 ± 0.05, T = 25.0 ± 0.2°C, shaking rate = 150 rpm. Adsorbent dosage 0.15 g/10 ml for raw-MWCNTs and 0.03 g/10 ml for SLS-MWCNTs.

3.2. Parameters optimization

3.2.1. Effect of adsorbent dosage

The effect of adsorbent dosage on removal efficiency for raw and SLS-MWCNTs was studied. The results are shown in Fig. 11. This was done by testing different adsorbent masses per 10 ml aliquots of Pb^{2+} solution. Other conditions such as initial metal concentration, pH, contact time, temperature and shaking speed were kept constant. The removal efficiency rise with adsorbent mass is due to the increase in available active adsorption sites. In the case of raw-MWCNTs, a small increase in removal efficiency was observed beyond 0.15 g/10 ml. Thus, this value was chosen as optimum dosage. In addition, removal efficiency was essentially constant using 0.03, 0.04 and 0.05 g/10 ml of the SLS-MWCNTs. Thus, optimum dosage of SLS-MWCNTs was chosen to be 0.03 g/10 ml. The optimum SLS-MWCNTs dosage is 5 times less than that for raw-MWCNTs. The removal efficiencies at optimum dosages are 53.9% and 95.9% for raw and SLS-MWCNTs, respectively.

3.2.2. Effect of contact time

Allowing sufficient contact time is essential for best adsorption results. The effect of contact time on removal efficiency was studied by changing the contact time in the range 5–120 min while keeping other parameters constant. Results are presented in Fig. 12, which shows that, for both raw and SLS-MWCNTs, most of the Pb^{2+} was adsorbed during the first 5 min. This can be attributed to the empty active sites available at the beginning of the process. At prolonged intervals, virtually all adsorption sites were occupied by Pb^{2+} and this explains the small increase in removal efficiency. Equilibrium was attained after 50 min for raw-MWCNTs and 30 min for SLS-MWCNTs.

3.2.3. Effect of pH

Pb^{2+}adsorption is sensitive to solution pH. This is because this ion exists in different forms depending on the pH of the solution. The predominant form of lead below pH 7 is Pb^{+2}. In the pH range 7–10, lead can precipitate in the form of $Pb(OH)_2$. Thus, within this pH range it is inaccurate to claim that lead removal is due to adsorption only [1]. Solutions with different pH, in the range 2–7, were pre-

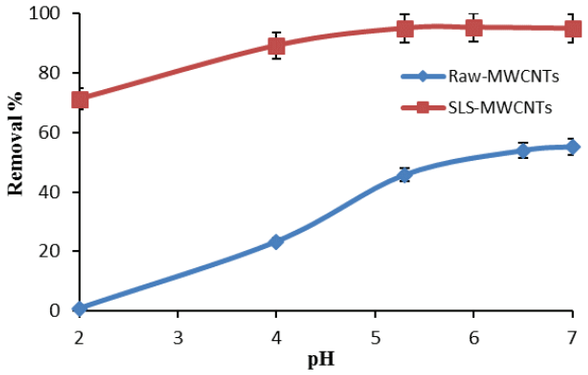

Fig. 13. Effect of pH on the removal of lead from aqueous solutions for both raw and SLS-MWCNTs. Initial [Pb^{2+}] = 100 ppm, T = 25.0 ± 0.2°C, shaking rate = 150 rpm. Raw-MWCNTs: adsorbent dosage = 0.15 g/10 ml, contact time = 50 min. SLS-MWCNTs: adsorbent dosage = 0.03 g/10 ml, contact time = 30 min.

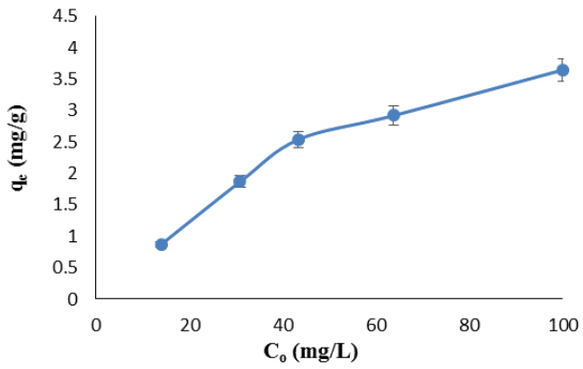

Fig. 14. Change in adsorption capacity with Pb^{2+} concentration using raw-MWCNTs at adsorbent dosage = 0.15 g/10 ml, contact time = 50 min, pH = 6.50 ± 0.05, T = 25.0 ± 0.2°C, shaking rate = 150 rpm.

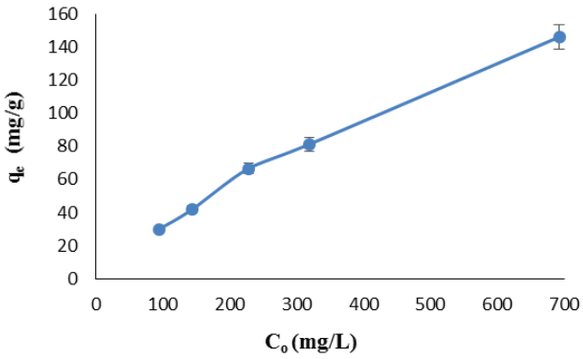

Fig. 15. Change in adsorption capacity with initial concentration using SLS-MWCNTs at adsorbent dosage = 0.03 g/10 ml, contact time = 30 min, pH = 5.3 ± 0.05, T = 25.0 ± 0.2°C, shaking rate = 150 rpm.

pared and the effect of pH on the removal efficiency was studied. Removal percentage as a function of solution pH for raw and SLS-MWCNTs is shown in Fig. 13. For both cases, removal efficiency increases with pH. This is probably due to the competition between H^+ and Pb^{2+} ions for adsorption sites. For raw-MWCNTs, the optimum pH was 6.5. Removal efficiency with SLS-MWCNTs was constant starting from pH 5.3, with further pH increases having no effect. Thus, pH 5.3 was chosen as the optimum pH of SLS-MWCNTs, with 95.1% removal. This compares with 45.8% removal using raw-MWCNTs at the same pH.

3.3. Adsorption isotherms

Information on adsorption equilibria can be valuable in predicting the effectiveness of adsorption [20]. Pb^{2+} solutions of different initial metal concentrations and with fixed pH, contact time, temperature and adsorbent dosage were used to study adsorption equilibrium. The equation used was:

$$q_e = \frac{(C_o - C_o) * V}{m} \tag{6}$$

where: q_e is the equilibrium adsorption capacity (mg/g), V is the volume of solution (ml) and m is the mass of adsorbent (g). Adsorption capacity as function of initial concentration as calculated from Eq. (6) is shown in Figs. 14 and 15 for raw and SLS-MWCNTs, respectively. The capacity using raw-MWCNTs at 100 ppm was 3.70 mg/g, compared to 30 mg/g using SLS-MWCNTs at the same concentration. This shows that the modification greatly enhances adsorption capacity.

The equilibrium data of raw and SLS-MWCNTs were fitted to four isotherms: Langmuir, Freundlich, Temkin and Dubinin-Radushkevich. Linear equations of these models are:

Langmuir model [21]:

$$\frac{C_e}{q_e} = \frac{C_e}{q_m} + \frac{1}{q_m K_L} \tag{7}$$

where q_m is maximum adsorption capacity (mg/g) and K_L is the Langmuir isotherm constant.

$$\log q_e = \log K_F + \frac{1}{n}\log C_e \tag{8}$$

where K_F is directly related to adsorption capacity and n to the intensity of adsorption.

Temkin model [22]:

$$q_e = \frac{RT}{b_T}\ln A_T + \frac{RT}{b_T}\ln C_e \tag{9}$$

where A_T is equilibrium binding constant (L/g) and b_T is the Temkin constant.

Dubinin-Radushkevich (D–R) model [22]:

$$\ln q_e = \ln q_s - K_{DR}\,\epsilon^2 \tag{10}$$

$$\epsilon = RT\ ln\left[1 + \frac{1}{C_e}\right] \tag{11}$$

where q_s is the theoretical isotherm saturation capacity (mg/g) and K_{DR} is the Dubinin–Radushkevich constant.

Results of data fitting on isotherm models for both raw and SLS-MWCNTs are given in Table 2. With a regression coeffi-

Table 2
Parameters for the four adsorption isotherm models for Pb^{2+} removal using raw and SLS-MWCNTs

Adsorption isotherm model	Parameters		R^2	
	Raw-MWCNTs	SLS-MWCNTs	Raw-MWCNTs	SLS-MWCNTs
Langmuir	q_m = 3.84 mg/g	q_m = 167 mg/g	0.99	0.96
	K_L = 0.29 L/mg	K_L = 0.021 L/mg		
Freundlich	n = 2.90	n = 2.50	0.88	0.97
	K_F = 1.10 ($mg^{1-1/n}\cdot L^{1/n}$)/g	K_F = 15.00 ($mg^{1-1/n}\cdot L^{1/n}$)/g		
Temkin	A_T = 10.00 L/g	A_T = 0.38 L/g	0.94	0.90
	B_T = 4200 mol/J	B_T = 86.00 mol/J		
Dubinin-Radushkevich	q_s = 3.20 mg/g	q_s = 78.00 mol^2/kJ^2	0.89	0.53
	K_{DR} = 1*10^{-6} mol^2/kJ^2	K_{DR} = 4*10^{-6} mg/g		

cient of 0.99, the Langmuir isotherm best describes the process, indicating monolayer and reversible adsorption of Pb^{2+} raw-MWCNTs [23]. The maximum adsorption capacity of raw-MWCNTs, as given by the Langmuir model, is 3.84 mg/g. By contrast, the Freundlich isotherm best describes adsorption on SLS-MWCNTs. K_F values for raw and SLS-MWCNTs are 1.1 and 15 g/mg, respectively. K_F is a measure of relative adsorption capacity of an adsorbent and thus SLS-MWCNTs have higher adsorption capacity [24]. Moreover, a 1/n value less than 1 points to favorable adsorption [22]. Adsorption capacity of SLS-MWCNTs was found to be 141 mg/g.

The adsorption capacities and removal times of different modified MWCNTs used in previous studies of Pb^{2+} removal from aqueous solutions are shown in Table 3. Wang et al. [5] used magnetic hydroxypropyl chitosan/oxidized multi walled carbon nanotubes (MHC/OMCNTs) composites as adsorbent. The maximum adsorption capacity in this study was 101.1 mg/g and the optimum contact time was 120 min. Moreover, Zhao et al. [7] compared removal of Pb^{2+}using raw MWCNTs to that using MWCNTs modified by TiO_2. The modification resulted in a large increase in adsorption capacity, from 33 to 137 mg/g. In the same study, the optimum contact time was found to be 60 min. Inspection of Table 3 reveals that the adsorbent used in this work has the highest adsorption capacity among those previously attempted, with a value of 141 mg/g, closely followed by the TiO_2 modified adsorbent. The lowest contact time (20 min) occurred with MWCNT modified with HNO_3 [12], followed by the SLS-MWCNT adsorbent used in this work (30 min).

Table 3
Adsorption capacities and contact times of various modified MWCNTs used for Pb^{2+} removal from aqueous solutions

Functional group	Adsorption capacity (mg/g)	Contact time (min)	Reference
Magnetic hydroxypropyl chitosan	101.1	120	[5]
Nitric acid	82	NA	[25]
2-vinylpyridine (VP)	37	NA	[6]
Oxygen-containing	40.79	90	[26]
Ethylenediamine	44.19	90	[26]
Diethylenetriamine	58.26	90	[26]
Titanium dioxide (TiO_2)	137	60	[7]
tris(2- aminoethyl) amine	43	45	[8]
1-isatin-3-thiosemicarbazone	14.56	60	[9]
Thiol	65.40	NA	[10]
Manganese oxide	78.74	120	[11]
Concentrated nitric acid	85	20	[12]
Sodium lauryl sulfate	141	30	This study

3.4. Adsorption kinetics

Adsorption kinetics provides information on adsorbate residence time and is thus of value for system design [27]. Pseudo-first order, pseudo-second order and Elovich models were used to study the adsorption kinetics of Pb^{2+} on raw and SLS-MWCNTs.

The linear form of the pseudo- first order equation given by Langergren and Svenska is [28,29]:

$$ln\ (q_e - q_t) = ln\ q_e - k_1\ t \quad (12)$$

where q_t and q_e are the amounts (mg) of adsorbate adsorbed per gram of adsorbent at time t and at equilibrium, respectively, k_1 is the Lagergren first order adsorption rate constant (min^{-1}), obtained from plotting $ln\ (q_e - q_t)$ *vs.* t.

The pseudo-second order kinetic model can be expressed by the following linear form [28,29]:

$$\frac{t}{q_t} = \frac{1}{k_2 q_e^2} + \frac{t}{q_e} \quad (13)$$

where k_2 is the second order adsorption rate constant (g/mg·min) which can be obtained from the intercept of the linear plot of t/q *vs.* t. The linear form of the Elovich model is [20]:

$$q_t = \frac{\ln\beta}{\alpha\beta} + \frac{\ln t}{\beta} \quad (14)$$

Table 4
Parameters for three adsorption kinetics models for Pb^{2+} removal using raw-MWCNTs

Adsorption kinetics model	Parameters		R^2	
	Raw-MWCNTs	SLS-MWCNTs	Raw-MWCNTs	SLS-MWCNTs
Pseudo-first order	k_1 = 0.038 min^{-1}	k_1 = 0.066 min^{-1}	0.94	0.92
Pseudo-second order	k_2 = 0.110 g/mg·min	k_2 = 0.055 g/mg·min	1.00	1.00
Elovich	α = 36000 mg/g·min	α = 5.00 * 10^9 mg/g·min	0.95	0.81
	β = 4.9 g/mg	β = 0.88 g/mg		

where α is the initial adsorption rate (mg/g·min) and β is the desorption constant (g/mg). Table 4 shows R^2 values and parameters of pseudo-first order, pseudo-second order and Elovich models for both raw and SLS-MWCNTs.

It can be seen that adsorption contact time data of both raw and SLS-MWCNTs are well fitted by the pseudo-second order model. R^2 values were found to be equal to 1 for both raw and SLS nanotubes. Thus, it can be concluded that Pb^{2+} uptake on the surface of both adsorbents is governed by the pseudo-second order rate equation with rate constants 0.11 and 0.055 g/mg·min, for raw and SLS-MWCNTs, respectively.

3.5. Adsorption mechanism

Adsorption involves three major steps: film diffusion, particle diffusion and adsorption. Since the last step is typically very fast, either film or particle diffusion will be limiting [28]. Adsorption models were used to determine the controlling step in the process. Liquid film and intra-particle diffusion models were applied to adsorption by raw and SLS-MWCNTs. The liquid film diffusion model can be expressed as follows [30]:

$$ln\,[1–F] = –K_{fd\,t} \quad (15)$$

$$F = \frac{q_t}{q_e} \quad (16)$$

where: K_{fd} is the liquid film diffusion constant. Data on raw and SLS-MWCNTs were fitted to this liquid film diffusion model (Fig. 16). Although, both plots show some linearity, neither passes through the origin, indicating that liquid film diffusion is not the limiting step in the process [30].

The intra-particle diffusion model is an empirical functional relationship based on theory developed by Weber and Morris. It can be expressed as follows [28]:

$$q_t = k_{id}\,t^{1/2} + C \quad (17)$$

where k_{id} is the intra-particle diffusion rate constant (mg/g·min), and k_{id} and C are the slope and the intercept of the linear plot of q_t vs $t^{1/2}$, respectively. Fig. 17 shows the results of the intra-particle diffusion model for raw and SLS-MWCNTs. Both plots do not pass through the origin, indicating that other mechanisms, beside intra-particle diffusion, contribute to the controlling step [29]. Moreover, the large value of the intercept in the case of SLS-MWCNTs indicates higher contribution of surface adsorption in the limiting step [30].

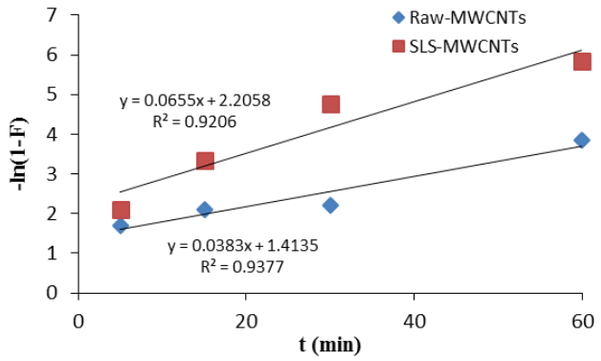

Fig. 16. Liquid film diffusion model for Pb^{2+} adsorption using raw and SLS-MWCNTs.

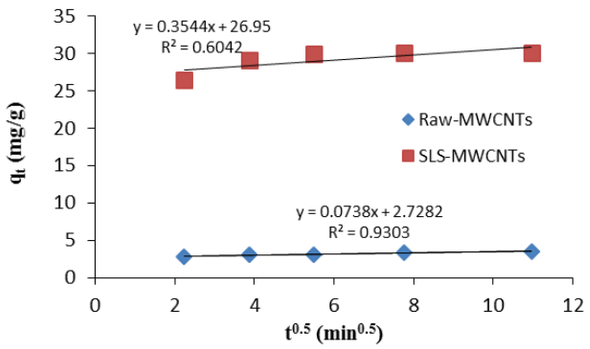

Fig. 17. Intra-particle diffusion model for Pb^{2+} adsorption using raw and SLS-MWCNTs.

3.6. Adsorption thermodynamics

The standard values of the apparent Gibbs free change (ΔG°\), apparent enthalpy (ΔH°\), and apparent entropy (ΔS°\), were calculated using Eqs. (18) and (19).

$$\Delta G^{\circ/} = \Delta H^{\circ/} - T\,\Delta S^{\circ/} \quad (18)$$

$$\ln K_c^{/} = \ln\left(\frac{Ca}{Ce}\right) = \frac{\Delta S^{\circ/}}{R} - \frac{\Delta H^{\circ/}}{RT} \quad (19)$$

where $K_c^{/}$ is the apparent equilibrium constant and C_a is the concentration of adsorbate on adsorbent at equilibrium (mg/L) [31,32]. The values of ΔG°/, ΔH°/ and ΔS°/ of raw and SLS-MWCNTs are given in Table 5. The positive

Table 5
Thermodynamic parameters for Pb^{2+} adsorption using raw-MWCNTs

Adsorbent	ΔG°\ (kJ/mol)			ΔH°\ (kJ/mol)	ΔS°\ (J/molK)
	298 K	308 K	318 K		
Raw-MWCNTs	–0.45	–0.79	–1.10	9.9	35
SLS-MWCNTs	–9.21	–7.80	–6.40	–51	–140

value of ΔH°/ with raw MWCNTs indicates an endothermic adsorption. By contrast, for SLS-MWCNTs, the negative ΔH°/ indicates an exothermic process [32]. This difference in behavior can be attributed to ion exchange in the case of raw-MWCNTs. The negative values of ΔG°/ indicate that adsorption is spontaneous [31]. Moreover, since all ΔG°/ values are small, (0 to –20 kJ/mol), it may be concluded that Pb^{2+} is physisorbed [33]. This is the case for both raw and SLS-MWCNTs. The sign of the entropy change gives information about the degree of freedom of the adsorbate. The positive ΔS°/ for raw-MWCNTs indicates an increase in the freedom associated with of Pb^{2+} adsorption, while the negative value for SLS-MWCNTs points to increased restriction [32].

3.7. Adsorption studies on the magnetite derivatives

Before using the magnetite pellets of SLS-MWCNTs in fixed bed column, they were tested in batch mode experiments. The effect of adsorbent dosage and contact time on the removal efficiency using magnetite SLS-MWCNTs (Mag. SLS-MWCNTs) and non-magnetite SLS-MWCNTs (SLS-MWCNTs) was studied. Figs. 18 and 19 show that the removal efficiencies of magnetite and non-magnetite SLS-MWCNTs, under the same conditions, are almost the same. Thus, magnetization has no effect on the efficiency of modified multi walled carbon nanotubes.

3.8. Packed bed column results

The first step in testing the efficiency of any new adsorbent is using it in a batch process. However, the batch method is not convenient in treating large scale wastewater; fixed bed adsorption columns are used instead. In column operation, the contaminated fluid is continuously fed through a bed packed with the adsorbent until it is fully loaded with the adsorbate.

Column experiments were carried out using the magnetite SLS-MWCNTs. Fig. 20 shows that results of the column operation expressed in terms of the change in C_t/C_o with time. It can be seen that C_t/C_o increases with time. This is because more volume of the contaminated fluid has passed through the column which exhausts it and loads it with the lead. The data collected from column operation were fitted to the Thomas, Yoon-Nelson, Adam–Bohart and the modified dose response (MDR) models. The experimental conditions were: height of the column (z): 2.0 cm, volumetric flow rate (Q): 1.0 ml/min, initial concentration (C_o): 100 ppm and velocity (U_o): 1.27 cm/min. These data, combined with the slopes and intercepts of experimental

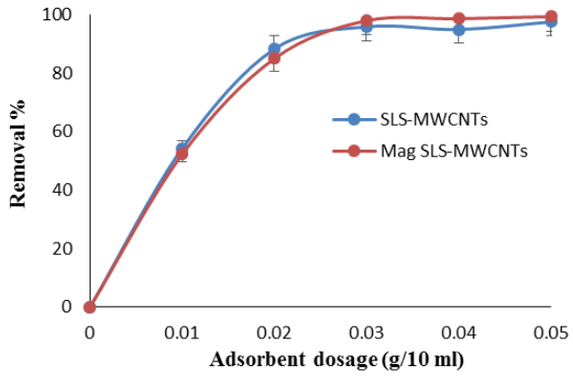

Fig. 18. Effect of adsorbent dosage on the removal of Pb^{2+} from aqueous solutions for magnetite and non-magnetite SLS-MWCNTs. Contact time = 120 min, pH = 5.30 ± 0.05, T = 25.0 ± 0.°C. Initial [Pb^{2+}] initial = 100 ppm, shaking rate = 150 rpm.

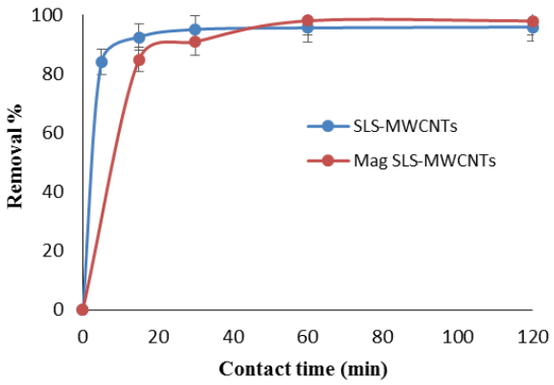

Fig. 19. Effect of contact time on the removal of Pb^{2+} lead from aqueous solutions for magnetite and non-magnetite SLS-MWCNTs. Adsorbent dosage = 0.03 g/10 ml, pH = 5.30 ± 0.05, T = 25.0 ± 0.2°C. Initial [Pb^{2+}] initial = 100 ppm, shaking rate = 150 rpm.

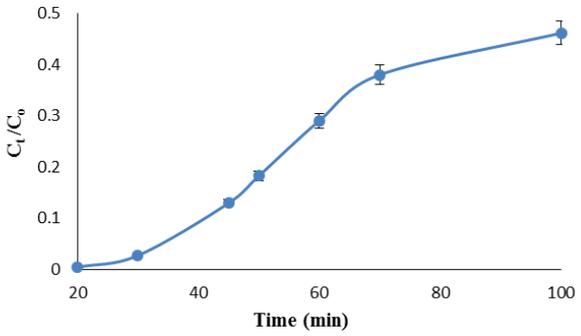

Fig. 20. Breakthrough curve of column operation at initial concentration = 100 ppm, pH = 5.30 ± 0.05, bed height = 2.0 cm, flow rate = 1.0 ml/min, T = 25.0 ± 0.2°C.

data fitting were used to calculate the parameters of the four models. Table 6, shows that MDR the best describes the data with $R^2 = 0.95$. By substituting MDR parameters in Eq. (5), it can be predicted that the column will reach 90% exhaustion after 160 min.

Table 6
Fixed bed column models parameters

Model	Parameters	R^2
Thomas	q (mg/g) = 28.00	0.79
	k_{Th} (ml/mg·min) = 0.64	
Yoon–Nelson	τ (min) = 85.00	0.79
	k_{YN} (min^{-1}) = 0.06	
Adam–Bohart	N_o (mg/L) = 6033	0.73
	k_{AB} (ml/mg·min) = 0.55	
MDR	q (mg/g) = 28.00	0.95
	a' (1/mg) = 3.50	

3.9. Regeneration attempts

Regeneration experiments on magnetite SLS-MWCNTs equilibrated with Pb^{2+} were carried out under optimum conditions. 0.7 M HNO_3 was added to the used adsorbent was shaken for 30 min in 0.7 M HNO_3 at 150 rpm and room temperature, followed by washing with DDW. The adsorbent was then vacuum-dried at 60°C for 24 h and reused in further adsorption-desorption cycles. In the first cycle, Pb^{2+} percentage removal dropped from 97.0 to 59.1 and in the second cycle from 59.1 to 33.6. These results lead to the conclusion that regeneration of SLS-MWCNT is inefficient.

4. Conclusion

Recently, carbon nanotubes have been employed extensively as new adsorbents for the removal of many pollutants. However, one of the main problems of carbon nanotubes is their tendency to agglomerate and form bundles in aqueous solutions. This reduces CNT dispersion and hence the surface area, thereby limiting available adsorption sites. To overcome these shortcomings, surface modification with SLS was applied to the pristine MWCNTs in order to obtain SLS-MWCNs. SLS-MWCNTs were characterized using SEM, EDS, TGA, FTIR, BET, and zeta potential, which also showed that the surface was successfully modified. Optimum values of adsorbent dosage, contact time and pH using raw-MWCNTs were 15.0 g/L, 50 min and 6.5, respectively. For SLS-MWCNTs, these were 3.00 g/L, 30 min and 5.3, respectively. The Langmuir isotherm best described raw-MWCNTs with 3.84 mg/g maximum capacity. The Freundlich isotherm best described SLS-MWCNTs with adsorption capacity of 141 mg/g at 700 ppm. Furthermore, kinetics studies revealed that both raw and SLS-MWCNTs followed the pseudo-second order kinetic model with rate constants 0.11 and 0.06 g/mg·min, respectively. Adsorption of Pb^{2+} by raw-MWCNTs was endothermic but that of SLS-MWCNTs was exothermic. However, Pb^{2+} was physisorbed on both surfaces. Magnetite pellets of SLS-MWCNTs were prepared, characterized using FTIR and used in batch experiments. Characterization showed that raw multi walled carbon nanotubes were successfully magnetized and modified with SLS. Batch adsorption results did not show any difference in removal efficiency between magnetite and non-magnetite SLS-MWCNTs. Magnetite pellets of SLS-MWCNTs were used in the packed column. Column operation modeling showed that MDR model was the best to describe the data with parameters q_{mdr} = 28.4 mg/g and a' = 3.47 mg^{-1}.

Acknowledgment

This work was supported by American University of Sharjah UAE. The authors would like to thank BDH Middle East L.L.C. for their help in running the zeta potential measurements.

References

[1] Ihsanullah, A. Abbas, A.M. Al-Amer, T. Laoui, M.J. Al-Marri, M.S. Nasser, M. Khraisheh, M.A. Atieh, Heavy metal removal from aqueous solution by advanced carbon nanotubes: critical review of adsorption applications, Sep. Purif. Technol., 157 (2015) 141–161.
[2] N.M. Mubarak, J.N. Sahu, E.C. Abdullah, N.S. Jayakumar, Removal of heavy metals from wastewater using carbon nanotubes, Sep. Purif. Rev., 43 (2013) 311–338.
[3] K.S. Ibrahim, Carbon nanotubes–properties and applications: a review, Carbon. Lett., 14 (2013) 131–144.
[4] V. Mittal, Surface Modification of Nanotube Fillers, Wiley-VCH, Weinheim, 2011.
[5] Y. Wang, L. Shi, L. Gao, Q. Wei, L. Cui, L. Hu, L. Yan, B. Du, The removal of lead ions from aqueous solution by using magnetic hydroxypropyl chitosan/oxidized multiwalled carbon nanotubes composites, J. Colloid. Interface Sci., 451 (2015) 7–14.
[6] X. Ren, D. Shao, G. Zhao, G. Sheng, J. Hu, S. Yang, X. Wang, Plasma induced multiwalled carbon nanotube grafted with 2-vinylpyridine for preconcentration of Pb(II) from aqueous solutions, Plasma. Process. Polym., 8 (2011) 589–598.
[7] X.W. Zhao, Q. Jia, N.Z. Song, W.H. Zhou, Y.S. Li, Adsorption of Pb(II) from an aqueous solution by titanium dioxide/carbon nanotube nanocomposites: kinetics, thermodynamics and isotherms, J. Chem. Eng. Data., 55 (2010) 4428–4433.
[8] M.S. Tehrani, P.A. Azar, P.E. Namin, S.M. Dehaghi, Removal of lead ions from wastewater using functionalized multiwalled carbon nanotubes with tris(2-aminoethyl) amine, J. Environ. Prot., 4 (2013) 529–536.
[9] M. Jahangiri, F. Kiani, H. Tahermansouri, A. Rajabalinezhad, The removal of lead ions from aqueous solutions by modified multi-walled carbon nanotubes with 1-isatin-3-thiosemicarbazone, J. Mol. Liq., 212 (2015) 219–226.
[10] C. Zhang, J.H. Sui, J. Li, Y.L. Tang, W. Cai, Efficient removal of heavy metal ions by thiol-functionalized super paramagnetic carbon nanotubes, Chem. Eng. J., 210 (2012) 45–52.
[11] S. Wang, W. Gong, X. Liu, Y. Yao, B. Gao, Q. Yue, Removal of lead(II) from aqueous solution by adsorption onto manganese oxide-coated carbon nanotubes, Sep. Purif. Technol., 58 (2007) 17–23.
[12] H.J. Wang, A.L. Zhou, F. Peng, H. Yu, L.F. Chen, Adsorption characteristic of acidified carbon nanotubes for heavy metal Pb (II) in aqueous solution, Mat. Sci. Eng. A-Struct., 466 (2007) 201–206.
[13] Y. Wang, L. Shi, L. Gao, Q. Wei, L. Cui, L. Hu, L. Yan, B. Du, The removal of lead ions from aqueous solution by using magnetic hydroxypropyl chitosan/oxidized multiwalled carbon nanotubes composites, J. Colloid Interface Sci., 451 (2015) 7–14.
[14] O. Kerkez-Kuyumcu, S.S. Bayazit, M.A. Salam, Antibiotic amoxicillin removal from aqueous solution using magnetically modified graphene nanoplatelets, J. Ind. Eng. Chem., 36 (2016) 198–205.
[15] Z. Xu, J.-G. Cai, B.-C. Pan, Mathematically modeling fixed-bed adsorption in aqueous systems, J. Zhejiang. Univ-Sc. A., 14 (2013) 155–176.

[16] A.P. Lim, A.Z. Aris, Continuous fixed-bed column study and adsorption modeling: removal of cadmium (II) and lead (II) ions in aqueous solution by dead calcareous skeletons, Biochem. Eng. J., 87 (2014) 50–61.
[17] P.R. Rout, R.R. Dash, P. Bhunia, Modelling and packed bed column studies on adsorptive removal of phosphate from aqueous solutions by a mixture of ground burnt patties and red soil, Adv. Environ. Res., 3 (2014) 231–251.
[18] B.H. Stuart, Infrared Spectroscopy: Fundamentals and Applications, Wiley, Chichester, 2008.
[19] M.A. Guzman, J.S. Salazar, R.O. Amaya, Y. Matsumoto, M.O. Lopez, Synthesis and Characterization of Magnetite-Graphene Oxide Nanocomposite, 13th International Conference on Electrical Engineering, Computing Science and Automatic Control (CCE), Mexico, 2016.
[20] S.M. Yakout, E. Elsherif, Batch kinetics, isotherm and thermodynamic studies of adsorption of strontium from aqueous solutions onto low cost rice-straw based carbons, Carbon. Sci. Tech., 1 (2010) 144–153.
[21] X. Chen, Modeling of experimental adsorption isotherm data, Information, 6 (2015) 14–22.
[22] A.O. Dada, A.P. Olalekan, A.M. Olatunya, O. DADA, Langmuir, Freundlich, Temkin and Dubinin–Radushkevich isotherms studies of equilibrium sorption of Zn^{+2} unto phosphoric acid modified rice husk, IOSR J. Appl. Chem., 3 (2012) 38–45.
[23] C.J. Geankoplis, Transport Processes and Unit Operations, Prentice-Hall International, New Jersey, 1993.
[24] N. Ghasemi, S. Mirali, M. Ghasemi, S. Mashhadi, M. Tarraf, Adsorption isotherms and kinetics studies for the removal of Pb(II) from Aqueous Solutions using Low-cost adsorbent, International Conference on Environment Science and Engineering IPCBEE, Singapore, 2012.
[25] Y.H. Li, J. Ding, Z. Luan, Z. Di, Y. Zhu, C. Xu, D. Wu, B. Wei, Competitive adsorption of Pb, Cu and Cd ions from aqueous solutions by multiwalled carbon nanotubes, J. Carbon., 41 (2003) 2787–2792.
[26] G.D. Vukovic, A.D. Marinkovic, S.D. Skapin, M.D. Ristic, R. Aleksic, A.A. Peric-Grujic, P.S. Uskoković, Removal of lead from water by amino modified multi-walled carbon nanotubes., Chem. Eng. J., 173 (2011) 855–865.
[27] Y.S. Ho, Review of second-order models for adsorption systems, J. Hazard. Mater., 136 (2006) 681–689.
[28] L.A. Tan, B.H Hameed, Adsorption isotherms, kinetics, thermodynamics and desorption studies of basic dye on activated carbon derived from oil palm empty fruit bunch, J. Appl. Sci., 10 (2010) 2565–2571.
[29] B.H. Hameed, D.K. Mahmoud, A.L. Ahmad, Equilibrium modeling and kinetic studies on the adsorption of basic dye by a low-cost adsorbent: coconut (cocosnucifera) bunch waste, J. Hazard. Mater., 158 (2008) 65–72.
[30] T. Tarawou, E. Young, Intraparticle and liquid film diffusion studies on the adsorption of Cu^{+2} and Pb^{+2} ions from aqueous solution using powdered cocoa pod (theobroma cacao), Int. Res. J. Eng. Technol., 2 (2015) 236–243.
[31] M. Dakiky, M. Khamis, A. Manassra, M. Mer'eb, Selective adsorption of chromium(VI) in industrial wastewater using low-cost abundantly available adsorbents, Adv. Environ. Res., 6 (2002) 533–540.
[32] M.A. Alanber, In: J.C. PirajÃ¡n, Thermodynamics: Interaction Studies - Solids, Liquids and Gases, InTech, Rijeka 2011, pp. 737–764.
[33] L. Largitte, R. Pasquier, A review of the kinetics adsorption models and their application to the adsorption of lead by an activated carbon, Chem. Eng. Res. Des., 109 (2016) 495–504.